A Novel Hyperspectral Salt Assessment Model for Weathering in Architectural Ruins

Yikang Ren[1,2], Fang Liu[1,2],

[1] School of Geomatics and Urban Information, Beijing University of Civil Engineering and Architecture, Beijing 102612, China - 2108570022072@stu.bucea.cn (Y.K.R.), lf@bucea.edu.cn (F.L.)

[2] Key laboratory of Modern Urban Surveying and Mapping, National Administration of Surveying, Mapping and Geoinformation, 102616, Beijing, China

(Commission II/WG6)

KEY WORDS: Architectural ruins,Weathering, Fractional order differentiation, Hyperspectral remote sensing, Machine learning

ABSTRACT:

The Dunhuang murals, a significant part of Chinese heritage, have suffered deterioration primarily due to environmental and chemical factors, notably salt damage. This study proposes a sophisticated method that synergizes Fractional Order Differentiation (FOD) and Partial Least Squares Regression (PLSR) to accurately invert the phosphate content in the Mural Plaster of the Dunhuang paintings. The focal points of the research include: 1) To address the issue of information loss and reduced modeling precision caused by integer order differentiation algorithms, the FOD method is employed for preprocessing hyperspectral data. This approach ensures the fine spectral differences in the phosphate content of the Mural Plaster are precisely captured, 2) Utilizing PLSR, the study models the spectral bands identified at a significance level of 0.01 with measured conductivity values, thereby enabling the precise prediction of the phosphate content in the murals. The research outcomes reveal: 1) The FOD method can elucidate the nonlinear characteristics and variation patterns of the mural samples in the hyperspectral curve.As the order increases from zero to two, the number of spectral bands meeting the 0.01 significance test initially decreases and then increases. The highest absolute value of the positive correlation coefficient is observed at 1.9 orders, corresponding to the 2077 nm band, 2) For predicting the phosphate content in the murals, the model at 1.9 orders is most suitable for inversion. This model, after cross-validation, achieves a maximum R^2 value of 0.783. This study created an efficient FOD-based model for estimating phosphate in mural plasters.

1. INTRODUCTION

The ancient mural sites serve as historical annotations, with the Dunhuang murals in China encapsulating the essence of contemporary human civilization and its developmental prowess, holding immense historical significance (Sun, Tongxin, et al., 2023; Wang, F., et al., 2022). Regrettably, due to the ravages of time, these murals have suffered from environmental impacts, resulting in fading, efflorescence, erosion by wind and sand, and mold damage. The detachment of the mural pigment layer from its mural plaster base, as well as the separation of the plaster layer from the cliff support layer, gravely diminishes the aesthetic and historical value of these murals (Sharma, et al., 2023; Scrivano, S., and Gaggero, L., 2020). Preserving these murals is tantamount to salvaging a civilization and art on the brink of extinction. Extensive research indicates that changes in the hydrothermal environment are a significant causative factor in the deterioration of mural paintings due to salt crystallization. Among existing methods for salt content analysis in mural samples, Spectrometer Diagnostics stands out as a non-contact, non-destructive technique (Li, D., et al., 2023). When studying salt content in murals, hyperspectral imaging can provide critical information on chemical composition, spatial distribution, quantity estimation, crystallization monitoring, environmental effects, and non-destructive testing, revealing these characteristics through spectral reflection and absorption (Peng, W., et al., 2022; Schodlok, M. C., et al., 2022; Ma, J., et al., 2022).

In summary, current hyperspectral remote sensing technology demonstrates some variability in the accuracy of its salinity predictions (Wang, Libing, et al. 2021).In the realm of hyperspectral data mining, mathematical differential transformation is a commonly employed strategy to enhance spectral band sensitivity. Scholars like Guozhou Qian (Guo Zhouqian, et al. 2023)have constructed spectral inversion models for sulfate in mural plaster utilizing first and second-order derivatives combined with salinity indices. Qing Zhong and others (Zhong,Q, et al. 2023) identified significant spectral feature enhancements using inverse first-order derivatives, establishing a hyperspectral prediction model for soil nickel content. Y. Hou and colleagues (Hou,Y and Zhang,F,2014) compared the modeling accuracy of simple linear regression, multiple linear stepwise regression, and PLSR with laboratory SOM content and hyperspectral data. They confirmed that second-order derivative PLSR was the optimal model, identifying the most sensitive wavelength range between 640-790 nm. However, current research indicates that first and second-order derivatives show significant differences from original data and tend to lose critical information affecting model accuracy (Fu,Cheng-Biao, et al. 2019).Fractional derivatives extend the concept of differentiation to any order, thereby providing a clearer depiction of the physical characteristics of natural systems (Sousa,J, et al. 2019;Zhou, P, et al. 2020).

Consequently, scholars have extensively studied the central issue of hyperspectral data preprocessing to establish higher-precision salt content prediction models. The fractional order differentiation model delineates the physical properties of systems in nature more clearly (Sousa,J et al. 2019). Compared to integer-order differentiation, fractional order differentiation provides a more precise model description and is widely applied in fields such as signal analysis, weather forecasting, and image processing (Abbas,S et al. 2017;Y. Yan et al. 2022). However, it was only in recent years that scientists began to apply fractional order differentiation models to the

preprocessing of soil hyperspectral data. Hong (Hong,Y et al. 2019) collected soil samples from the Han River Plain in Wuhan and computed the fractional order differentiation of the soil spectra, ranging from 0.0 to 2.0 order in 0.25 order intervals. Wang (Wang,X et al. 2018) focused on saline soils in the National Nature Reserve of the Ebinur Lake Wetland in Xinjiang for quantitative prediction of organic matter content. Simulation results indicated the highest precision in organic matter quantification at a model order of 1.2. Recent studies have found that fractional order differentiation methods can more meticulously depict the variations in the hyperspectral reflectance of Mural Plaster samples, thereby uncovering more hidden information and enhancing the precision of inversion models.

Based on the aforementioned analysis, scholars have made considerable efforts and explorations using the FOD method for the quantitative inversion of salt content in hyperspectral remote sensing.(Abbas,S et al. 2017;Y. Yan et al. 2022;Wang,X et al. 2018). However, the majority typically only employ conventional integer-order differentiation and spectral transformation processing when selecting salt-sensitive bands in ancient mural plaster. Whether fractional order differentiation can innovatively be applied to extract the salt content characteristics of saline mural surfaces, and more intricately delineate the changes in reflectance of the ancient mural plaster, to extract more hidden information from the hyperspectral reflectance curves and improve the precision of inversion models remains to be verified in this empirical study. Figure 1 illustrates the salt migration and phase transition mechanisms in the in-situ environment of the mural.

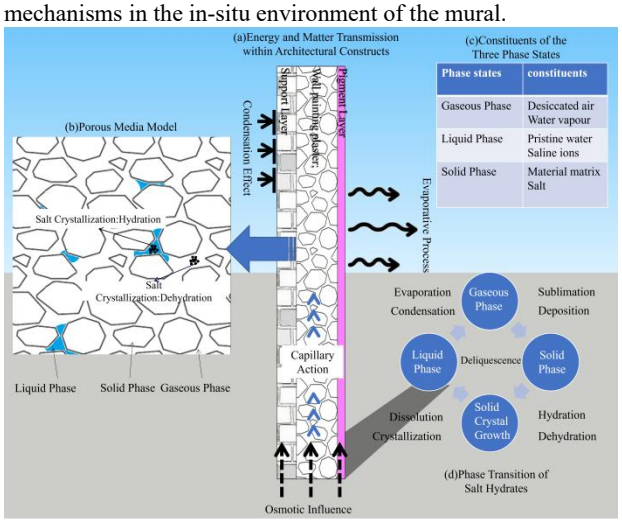

Figure.1 Illustration of the in-situ environmental conditions of murals, focusing on the hydrothermal transport of salts, porous medium models, and phase transition mechanisms.

2. EXPERIMENT AREA AND SAMPLE PREPARATION

This study focuses on ancient murals at the Mogao Caves in Dunhuang, selected for their significant historical value and characteristic salt damage. The research reveals various forms of salt-induced deterioration, including: (i) efflorescence, where salt crystallizes on the mural's surface, commonly referred to as "white frost," directly affecting the mural's visual and physical properties; (ii) friability, where the mural plaster becomes loose due to the action of soluble salts, compromising the structural integrity of the mural; (iii) fissures, indicating displacement and cracking of the mural, with salt expansion being a key factor in the formation or worsening of these cracks; (iv) craquelure, characterized by fine, net-like cracks on the mural surface, highlighting the subtle effects of salt content fluctuations on the mural's texture. These manifestations of salt damage not only focus on quantitative analysis of salt content but also delve into how salt, through various physical and chemical reactions, leads to diverse forms of degradation in murals, emphasizing the importance of in-depth salt content analysis to improve our understanding and mitigation of these impacts.

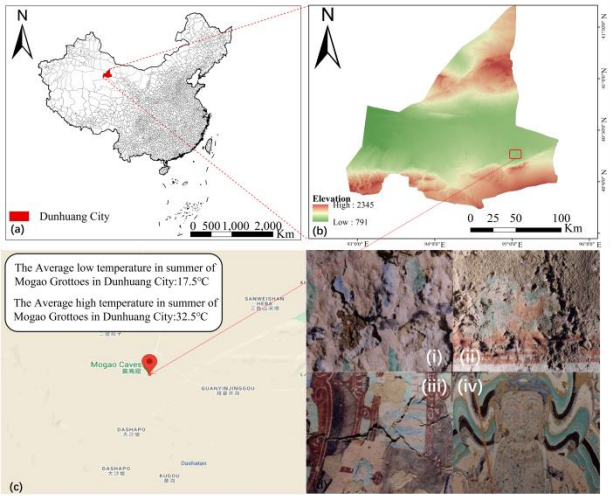

Figure 2. (a)- (c) depict an overview of the research area. (d) sh owcases typical pathological types found in mural paintings of t he study area: (i)Salt efflorescence, (ii)Alkaline effervescence, (iii) Fissures, (iv) Crazing.

The method of sample preparation was based on the studies described in reference (Bi,W, 2022),while the desalination process adhered to the GB/T50123-2019 standard.Table 1 presents a list of materials used in the experiment.

component	Material ratio (wt%)			
	Chengban soil	Sand	Wheat straw	Water
Coarse plaster	64	36	3	20

Table 1. Inventory of Experimental Materials.

3. DATA SOURCE AND METHODOLOGY

3.1 Data Collection

The aim of this experiment is to utilize hyperspectral technology for the non-contact diagnosis of salt content on the surface of Mural Plaster materials and to construct a pertinent model.First,design and prepare five sets of Mural Plaster samples with varying concentrations (a total of 50 pieces), and to collect their hyperspectral data. The methodology for sample preparation was informed by the study conducted by (Bi,W. 2022), while the desalination process adheres to the GB/T50123-2019 standard.Initially, the raw materials used for sample preparation, including kaolin clay, sand, and wheat straw, undergo a desalination process. Subsequently, the desalinated soil samples are dried, crushed, and sieved for future use. The treated kaolin clay, sand, and wheat straw are mixed in a mass ratio of 64:36:3, to which 20% of the total solid mass of distilled water is added. Following this, the material is prepared for molding. The homogenously mixed materials are filled into molds using a spreading technique to ensure a smooth surface, and vibration is applied to expel any excess air within the specimens. The samples are then placed in an oven and baked at 90°C for 2 hours to achieve a state as dry

as possible. This temperature is chosen to minimize the moisture content within the samples, approximating a completely dry condition.

The next step involved preparing five different concentrations of dodecahydrate disodium hydrogen phosphate solutions, specifically at 0.608 mol/L, 0.808 mol/L, 1.008 mol/L, 1.208 mol/L, and 1.408 mol/L. These solutions represented a gradient of erosive conditions from the lowest to the highest, sequentially termed as minimal concentration erosion, low concentration erosion, medium concentration erosion, high concentration erosion, and maximal concentration erosion. Temperature control was maintained using a THD-0506/1015 high-precision low-temperature constant temperature water bath. The mural plaster samples were immersion exposed to different concentrations of the dodecahydrate disodium hydrogen phosphate solution at 32.5°C through capillary action, simulating the real-world capillary absorption effect of Mural Plaster from groundwater seepage. Subsequently, the samples were thoroughly air-dried at room temperature, and their surface spectral reflectance was measured using an ASD-FieldSpec4HI-RES terrestrial spectrometer(The spectral range spans from 350 to 2500 nm, with a sampling interval of 1.4 nm between 350 and 1000 nm, and 2 nm from 1001 to 2500 nm). Figure 3 illustrates the experimental layout and procedural flow, as well as the method of collecting hyperspectral data for Mural Plaster.

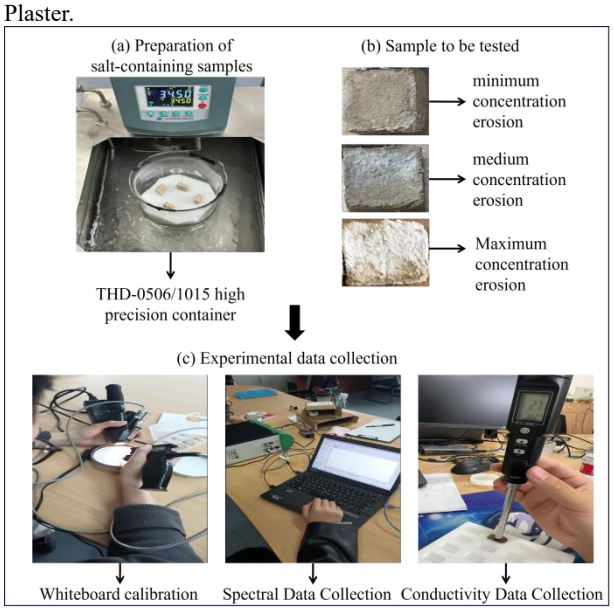

Figure 3.Preparation of samples and collection of hyperspectral data for Mural Plaster.

3.2 Statistical Analysis of Electrical Conductivity Data in Mural Plaster

The coefficient of variation is employed to articulate the degree of relative fluctuation or dispersion in conductivity measurement values.The electrical conductivity data of Mural Plaster collected under the five different conditions were statistically described using data density distribution, mean, standard deviation (SD), minimum value (Min), first quartile (Q1), third quartile (Q3), and coefficient of variation (CV). The first and third quartiles (Q1 and Q3) are indicated with red dashed lines, while the mean is denoted with a blue dashed line. OC1 to OC5 represent the five conditions ranging from minimal to maximal concentration erosion. The coefficient of variation (CV), also known as the dispersion coefficient, is a standardized measure of the dispersion of a probability distribution, defined as the ratio of the data's standard deviation to its mean. Data is considered to have low concentration variability when CV ≤ 15%, moderate variability when 15% < CV ≤ 35%, and high variability when CV > 35%. The formula for calculating the coefficient of variation (CV) is as follows(J. Zhang, et al. 2023):

$$CV = \frac{\sigma}{u} \times 100\% \tag{1}$$

where CV = the coefficient of variation (expressed as a percentage)
σ = the standard deviation of the sample
u = the mean value of the sample

3.3 Preliminary Processing of Hyperspectral Data

Initially, the spectral reflectance data for mural plasters was cleansed of low signal-to-noise ratio bands between 350-399nm and 2401-2500nm. Following this, the Savitzky-Golay filter was applied to smooth the hyperspectral reflectance data of 100 simulated plaster layer samples(J. Chen, et al. 2004), utilizing 21 window points and a second-order polynomial (Guo Zhouqian, et al. 2023).

$$y_i^{'} = \frac{1}{\Delta} \sum_{j=-m}^{m} c_j \cdot y_{i+j} \tag{2}$$

where $y_i^{'}$ = the spectral reflectance at position i after smoothing.
y_{i+j} = points within the original data series.
c_j = coefficients in the convolution kernel, acquired through polynomial fitting.
m = half the size of the window.
Δ = hypically 1, unless the intervals between data points are non-uniform.

3.4 Research Methodology

3.4.1 Grünwald-Letnikov Fractional Differentiation Fractional Order Differentiation (FOD) represents an extension of traditional integer-order differentiation and manifests in various forms within the realms of mathematics and engineering (Karaca, Yeliz, and Dumitru Baleanu. 2022), such as Riemann-Liouville (R-L), Lévy, Weyl, Caputo, and Grünwald-Letnikov (G-L) (Wang, X et al. 2020). The current experiment employs the Grünwald-Letnikov method, which, owing to its discrete nature, is particularly suitable for the numerical computation of hyperspectral signals (Equation 3),Γdenotes the Gamma function ($\Gamma(v) = (v-1)!$).

$$d^{v} f(x) = \lim_{h \to 0} \frac{1}{h^{v}} \sum_{n=0}^{[(t-a)/h]} (-1)^{n} \frac{\Gamma(v+1)}{n!\,\Gamma(v-n+1)} f(x - nh) \tag{3}$$

where v = the fractional order
h = step size
t and a = upper and lower bounds of FOD

In this experiment, assuming the function f (x) as a one-dimensional hyperspectral signal with a band range of [a, t], where x ∈ [a, t] divided by the differential step length h. Given that the ASD FieldSpec® 3 Hi-Res Spectrometer's retention interval is 1nm, the differential step length can be set to h=1. Consequently, the expression for the v-th order fractional differentiation of the function f (x) can be derived from Equation (3) as follows(Wang,X et al. 2018):

$$\frac{d^{v} f(x)}{dx^{v}} \approx f(x) + (-v) f(x-1) + \frac{(-v)(-v+1)}{2} f(x-2) + \frac{(-v)(-v+1)(-v+2)}{6} f(x-3) + \ldots + \frac{\Gamma(-v+1)}{n!\,\Gamma(-v+n+1)} f(x-n) \quad (4)$$

where v = the fractional order
x = the wavelength

3.4.2 Modeling PLSR In this study, the objective is to establish an inversion model to explore the relationship between conductivity of Mural Plaster and spectrally significant bands using machine learning method.A Partial Least Squares regression model was employed to construct the model as delineated in Equations 5 and 6 (Figure 4)(Mehmood, et al. 2020).

$$X = T \times P^{T} + E \quad (5)$$

$$Y = U \times Q^{T} + F \quad (6)$$

where X = Spectral bands ascertained through significance testing
Y = The conductivity of Mural Plaster
T = Score matrix for explanatory variables
U = Score matrix for response variables
P = Loading matrix for explanatory variables
Q = Loading matrix for response variables
E and F = Residual matrix

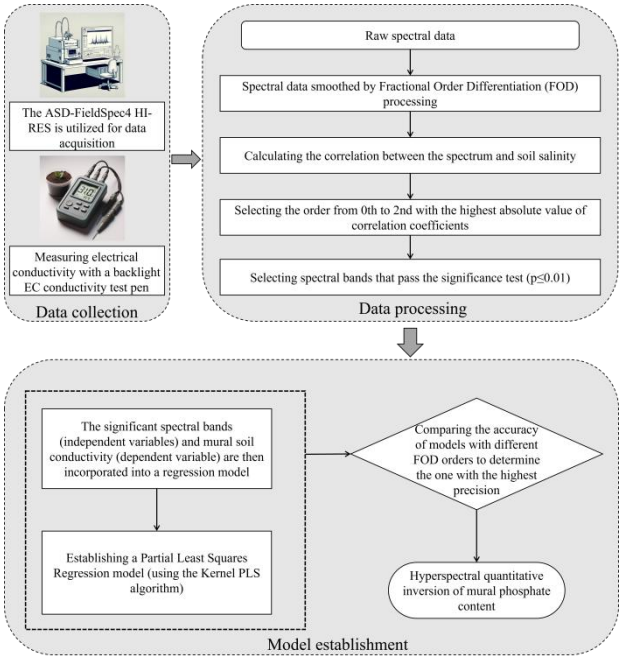

Figure 4.Workflow of the FOD-PLSR method.

3.4.3 Evaluation This paper employs-accuracy assessment metrics to evaluate the efficacy of the predictive modeling (Tian, A et al. 2021;Zhang,J et al. 2023). The computation formulas for R^2, RMSE (Root Mean Square Error), and MAE (Mean Absolute Error) are delineated as follows in Equations (7) to (9).

$$R^{2} = \left(\frac{\sum_{i=1}^{n} \left(y_i - \bar{y}\right)\left(z_i - \bar{z}\right)}{\sqrt{\sum_{i=1}^{n} \left(y_i - \bar{y}\right)^{2} \cdot \sum_{i=1}^{n} \left(z_i - \bar{z}\right)^{2}}} \right)^{2} \quad (7)$$

$$RMSE = \sqrt{\frac{\sum_{i=1}^{n} \left(y_i - z_i\right)^{2}}{n}} \quad (8)$$

$$MAE = \frac{1}{n} \sum_{i=1}^{n} \left| y_i - \hat{y}_i \right| \quad (9)$$

where n = the number of mural plaster samples
y_i = the EC measurement value of the *i*-th mural plaster sample
$\bar{y}$ = the average value of the measured values of all mural plaster samples
z_i = the predicted EC value of the i-th mural plaster sample
$\bar{z}$ = the average EC predicted value of all mural floor samples

The coefficient of determination of the calibration data set is expressed as R_c^2. The root mean square error of the calibration data set and the validation data set is expressed as $RMSE_c$ and $RMSE_v$. The coefficient of determination of the validation data set is expressed as R_v^2, and the performance of the model is expressed as MAE. Among them, R^2 is used to evaluate the model fitting degree. The closer the value is to 1, the higher the model accuracy. RMSE and MAE are used to evaluate the stability of the model. The closer the value is to 0, the better the RMSE and MAE are.

4. RESULTS

4.1 Statistical Description of Mural Plaster Electrical Conductivity

As depicted in Figure 5,The electrical conductivity values of Mural Plaster samples are a direct reflection of the variations in salt content within the same material, exhibiting certain variability. Statistical analysis reveals that the sample values ranged from 2.27 $ms \cdot m^{-1}$ to 4.86 $ms \cdot m^{-1}$. The average and standard deviation of the EC values were found to be 3.55 ± 0.75 $ms \cdot m^{-1}$. The first (Q1) and third (Q3) quartiles of the data are 2.98 $ms \cdot m^{-1}$ and 4.15 $ms \cdot m^{-1}$, respectively, indicating that 50% of the sample EC values fall between these two figures. Furthermore, the Coefficient of Variation (CV), derived using Equation (1), is 21%, signifying a moderate level of relative variability in the EC values of the samples.

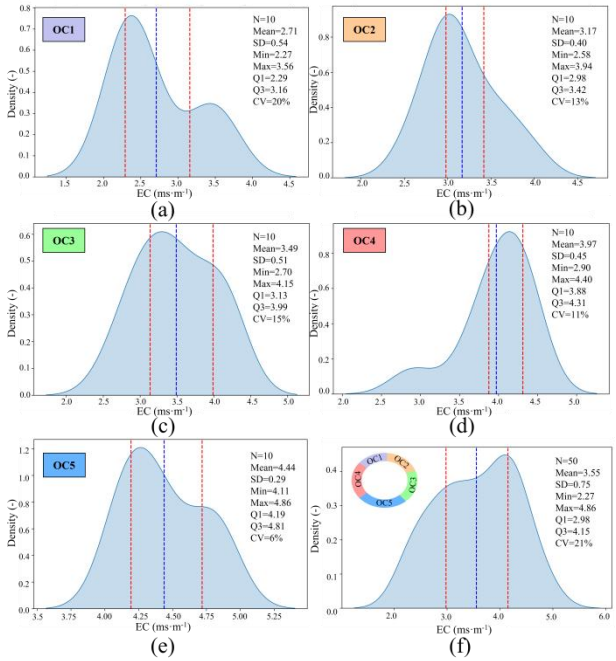

Figure 5.Statistical description of the Electrical Conductivity (EC) values in Mural Plaster.

4.2 Hyperspectral Characteristics of Simulated Mural Plaster under Different Salt Concentration Erosion

Based on Equation 2, the spectral data are smoothed to highlight these spectral features. As observed in Figure 6, the reflectance spectra of Mural Plaster, subjected to varying concentrations of salt erosion, exhibit similar shapes. The colored curve represents the average spectrum of the Mural Plaster samples. Within the 400-2400 nm wavelength range, shows reflectance values between 0.08 and 0.45, displaying notable fluctuations.

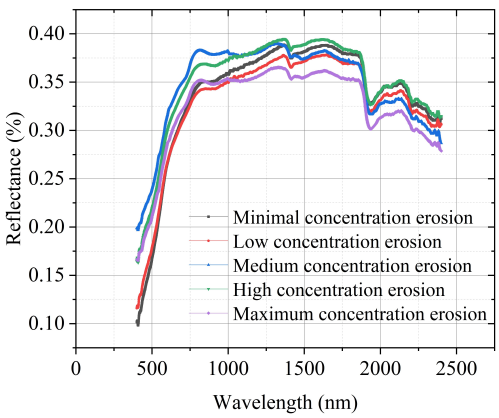

Figure 6. Spectral reflectance curves of mural samples under different conditions.

4.3 Fractional Order Differentiation Results of Spectral Curves

Given the rich high-dimensional information in hyperspectral data and the difficulty in capturing sensitive bands and features (Song, G et al. 2023), the FOD calculation method delineated in Section 3.4.1 was utilized on the samples, employing Equation (4) to enhance the analysis. This method allows for the control of differential step length, thereby enhancing the accuracy of salt content detection. Following the approach of (Zhang,J et al. 2023), the interval and step length were set at [0-2] and 0.1, respectively. Figure 7 illustrates the average spectrum of the Mural Plaster samples.

The results indicate that as the order increases from 0 to 2, the difference in spectral reflectance enlarges, and the differential values progressively approach zero, explainable by the mathematical theory of the G-L method. Given the presence of peaks and valleys of certain widths in the reflectance, when the sampling step length is less than these widths, this difference is amplified during computation, thus enhancing spectral information. Inevitably, differentiation operations introduce noise significantly different from adjacent bands, or amplify short interval reflectance peaks and valleys, subsequently introducing high-frequency noise (Zhang,J et al. 2023). Therefore, at 0.1-0.9 order, the extremities of band peaks, valleys, and inflection points are maximally extracted. At 1.0 order, the reflectance corresponding to the full spectral wavelength drops below 0.1, while at 0.5 order, it fluctuates around zero, beginning to show negative values.

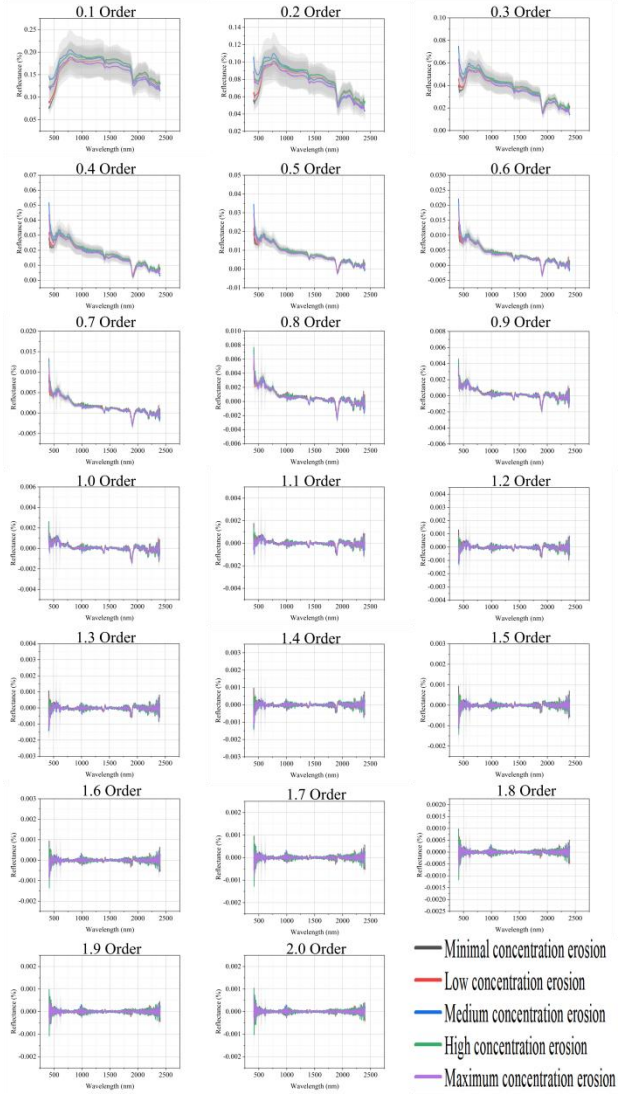

Figure 7. Average fractional-order derivative spectra of Mural Plaster samples. The range of orders spans from 0 to 2, with a step size of 0.1. Colored curves represent the average spectra of Mural Plaster samples, while the gray shadow indicates their standard deviation.

4.4 The Correlation between Fractional Order Derivative (FOD) Results and Salt Content

The optimal correlation between fractional order differential spectra and the phosphate content of Mural Plaster, along with corresponding spectral bands, is presented in Table 2.

Differential order	0.1	0.2	0.3	0.4	0.5
Correlation coefficient	0.509	0.512	0.515	0.518	0.522
Wavelength (nm)	408	408	408	408	408
Differential order	0.6	0.7	0.8	0.9	1
Correlation coefficient	0.526	0.526	0.512	−0.527	−0.606
Wavelength (nm)	408	408	401	874	874
Differential order	1.1	1.2	1.3	1.4	1.5
Correlation coefficient	−0.633	−0.619	−0.579	−0.556	−0.539
Wavelength (nm)	847	847	874	874	2064
Differential order	1.6	1.7	1.8	1.9	2
Correlation coefficient	−0.544	−0.543	0.549	0.552	0.543
Wavelength (nm)	2064	2064	2077	2077	2239

Table 2. Optimal Correlation between the Fractional Order Differential Spectra and Phosphate Content in Mural Plaster, Along with Corresponding Spectral Bands

Correlation coefficients provide an intuitive reflection of the linear relationship between spectral reflectance and phosphate content in Mural Plaster. The higher the correlation, the more sensitive the spectral response, which in turn improves the predictive accuracy of subsequent models. Figure 8 illustrates the correlation coefficients between differential spectral orders and the severity of the disease. It reveals that the correlation between different orders of differential spectra and phosphate content in Mural Plaster varies significantly. Within these differential spectra, one can observe different patterns of correlation with the phosphate content in Mural Plaster.

The correlation coefficient can intuitively reflect the linear correlation between spectral reflectance and the phosphate content of Mural Plaster; a higher correlation signifies a more sensitive spectral response, which in turn suggests more accurate predictive modeling outcomes.The correlation coefficients of the various orders of differential spectra and the severity of the pathology are as depicted in Figure 8.Figure 8 elucidates the significant differences in the correlation between the differential spectra of varying orders and the phosphate content of the Mural Plaster. Within these differential spectra of different orders, one can observe distinct patterns of correlation with the phosphate content of the Mural Plaster.Initially, it is noticeable that the maximum absolute values of the correlation coefficients fluctuate minimally and follow a similar trend from 0.1 to 0.7 order.In the visible light region (approximately 400 - 700 nm) and the near-infrared region (700 - 2500 nm), the correlation coefficients transition from positive to negative as the order increases.Furthermore, the adjacent bands of the correlation coefficients exhibit considerable volatility, becoming increasingly chaotic, which indicates that higher-order differentials capture more complex non-linear relationships.Lastly, the Mural Plaster phosphate has several advantageous wavelength ranges: 400-490 nm, 790-820 nm, 840-890 nm, 1150-1170 nm, 1380-1390 nm, 1465-1480 nm, 1760-1790 nm, 2060-2090 nm, 2190-2210 nm, and 2240-2290 nm. As the order incrementally rises from zero to first order, the overall trend of the number of bands that satisfy the 0.01 significance level test under spectral transformation is to initially decrease and then increase with the order.Based on the data presented in Table 2, it can be discerned that the maximum absolute value of the positive correlation coefficient is observed at the 1.9 order, corresponding to a wavelength of 2077 nm. Conversely, the peak absolute value of the negative correlation coefficient occurs at the 1.1 order, with the associated wavelength being 847 nm.Its first six characteristic bands (2077, 2064, 1470, 402, 1786, and 1712 nm) exhibit high consistency with the advantageous wavelength ranges of the Mural Plaster phosphate.In contrast, the characteristic bands extracted at integer orders (1.0 and 2.0 orders), although partially coinciding at 1.0 order (874, 847, 848, 854, 850, 875, and 2239 nm), differ significantly at 2.0 order (2239, 1180, 1605, 1756, 2063, and 1793 nm).This suggests that fractional-order differentiation is more effective in capturing spectral characteristics related to the phosphate content of Mural Plaster.

In conclusion, when establishing a spectral inversion model for Mural Plaster phosphate, 1.9 order differential spectral analysis may be the optimal choice.However, to ensure the accuracy and reliability of the model, it is still necessary to conduct a comprehensive comparison, considering the results of different orders of differential spectral analysis, as well as their capability in revealing the relationship between spectral reflectance and plaster phosphate content.

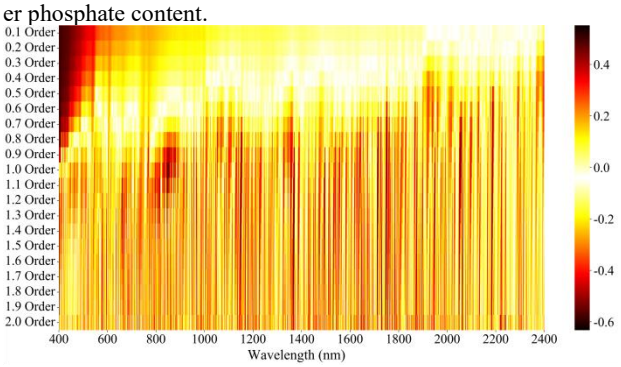

Figure 8. Correlation coefficients between differential spectra at different orders and the phosphate content in Mural Plaster.

4.5 Model Construction of Mural Plaster Phosphate Monitoring from Feature Bands Extracted by the FOD Algorithm

Order	Number of bands	Calibration Dataset			Validation Dataset		
		MAE_c	R_v^2	$RMSE_c$	MAE_v	R_v^2	$RMSE_v$
0.1	110	0.431	0.509	0.498	0.453	0.485	0.527
0.2	96	0.431	0.511	0.498	0.456	0.475	0.531
0.3	91	0.433	0.511	0.498	0.456	0.454	0.537
0.4	76	0.421	0.496	0.499	0.451	0.471	0.534
0.5	71	0.349	0.638	0.426	0.426	0.557	0.516
0.6	69	0.395	0.629	0.442	0.456	0.549	0.506
0.7	84	0.284	0.739	0.368	0.456	0.561	0.475
0.8	110	0.281	0.752	0.362	0.342	0.676	0.439
0.9	171	0.229	0.820	0.303	0.337	0.714	0.413
1	205	0.167	0.913	0.217	0.323	0.716	0.393
1.1	225	0.134	0.943	0.174	0.320	0.706	0.412
1.2	220	0.103	0.766	0.129	0.304	0.729	0.381
1.3	204	0.121	0.956	0.157	0.321	0.743	0.387
1.4	194	0.111	0.958	0.142	0.303	0.733	0.377
1.5	178	0.159	0.953	0.156	0.363	0.685	0.416
1.6	176	0.174	0.968	0.131	0.404	0.673	0.429
1.7	169	0.248	0.884	0.255	0.426	0.580	0.478
1.8	161	0.191	0.918	0.209	0.382	0.708	0.422
1.9	163	0.078	0.984	0.057	0.312	0.783	0.371
2	162	0.089	0.978	0.109	0.392	0.561	0.467

Table 3. Monitoring Models and Validation Results for Phosphate Content in Mural Plaster

Utilizing Equations 5 and 6, Table 3 can be derived.According to Table 3, the model exhibits varying performance at different orders. In integer-order differentiation, the first-order differential spectrum model has a higher coefficient of determination R^2 than the second order, with the highest R^2 of 0.716 in the validation set, indicating greater accuracy. In fractional order differentiation, model performance varies with the refinement of the differentiation order, achieving an optimal R^2 of 0.783 at 1.9 order, surpassing both the original and second-order spectra. Additionally, the fractional order differentiation at 1.9 order yields RM

SE and MAE values of 0.057 and 0.078 in the calibration set, a nd 0.371 and 0.312 in the validation set, respectively, demonstr ating high predictive accuracy and stability.

Figure 9 presents the optimal Mural Plaster Phosphate Monitori ng Models established based on sensitive bands selected from F OD spectra, including (a) 1.0 order, (b) 2.0 order, (c) 1.1 order, and (d) 1.9 order models.

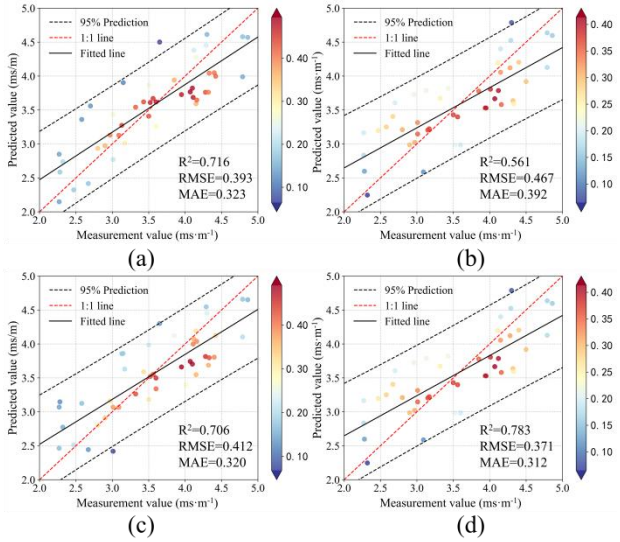

Figure 9. Optimal Mural Plaster phosphate monitoring models established based on FOD spectral band selection: (a) 1.0 order, (b) 2.0 order, (c) 1.1 order, (d) 1.9 order.

A comparison of model performance reveals that the 1.9 order differential spectrum model exhibits the best performance in th e calibration dataset, with an R^2 of 0.984 and RMSE of 0.057. I ts performance in the validation dataset is also superior, with an R^2 of 0.783 and RMSE of 0.371, demonstrating its high accura cy and reliability in monitoring phosphate content in Mural Pla ster.

5. DISUSSION

The innovations of this study are as follows:

(1) In terms of spectral preprocessing, this study innovatively p roposed the Fractional Order Differentiation (FOD) method for preprocessing the hyperspectral data of Dunhuang Mural Plaste r layers. Compared to traditional integer-order differentiation al gorithms, the FOD method more acutely captures minor variati ons in phosphate content within hyperspectral data. By unveilin g the nonlinear characteristics and complex patterns of variatio n in the mural samples' spectra, FOD preprocessing retains mor e nuanced information, significantly enhancing the accuracy an d reliability of modeling for Mural Plaster phosphate content.

(2) On feature band extraction and modeling, the research has d eveloped a model combining Fractional Order Differentiation a nd Partial Least Squares Regression (FOD-PLSR) for the hyper spectral feature inversion of Mural Plaster phosphate content. T his enables non-destructive detection and accurate prediction of phosphate content in Dunhuang Mural Plaster, which holds sig nificant value for cultural heritage conservation.

However, it is pertinent to acknowledge the limitations of this s tudy. In selecting sensitive features for Mural Plaster phosphate, only the selection of sensitive bands was considered, without e xploring combinations of sensitive bands, such as the constructi on of salinity indices at different orders. Moreover, the study o nly employed a limited range of fractional orders with a step le ngth of 0.1, without analyzing the impact of more detailed fract ional order differential spectral changes on the remote sensing monitoring of Mural Plaster phosphate damage. Furthermore, t he current study primarily focuses on mural salt damage monito ring under specific samples and conditions, potentially limiting the model's generalizability across different types of murals or environmental conditions. Future research should consider a br oader range of samples and diverse environmental conditions to enhance the applicability of the model. Future studies should f ocus on improving the model's generalizability, optimizing algo rithms and automation of technologies, and exploring the applic ation of these techniques in other related fields. Through these efforts, further advancement of hyperspectral technology in cult ural heritage conservation and other related areas can be achiev ed.

6. CONCLUSION

This study has processed hyperspectral data using the Fractiona l Order Differentiation (FOD) method, delving into the sensitiv e orders and characteristic bands between spectral reflectance a nd phosphate concentration in Mural Plaster under various conc entration erosion conditions. Furthermore, we developed an FO D-PLSR model based on fractional order differential spectra, ai med at precisely estimating the phosphate content in Mural Plas ter.

(1) Trends in the Correlation Coefficients between FOD Fractio nal Orders and Salt Content: Sensitive bands for phosphate cont ent variations are identified at 408, 847, 874, 2064, and 2077 n m (Table 2).

(2) Correlation between Spectral Reflectance and Phosphate Co ncentration: The FOD method reveals the nonlinear characterist ics and patterns of change in the hyperspectral data of mural sa mples. The spectral sensitivity, controlled by the weighted orde r, shows a trend of initially increasing and then decreasing in th e number of spectral bands satisfying the 0.01 significance test as the order increases from zero to one. The highest absolute va lue of positive correlation occurs at 1.9 order, corresponding to the 2077 nm band (Figure 8, Table 2), with its top six character istic bands (2077, 2064, 1470, 402, 1786, and 1712 nm) showin g high consistency with known sensitive bands. In contrast, the characteristic bands extracted at integer orders (1.0 and 2.0) par tially align at 1.0 order (874, 847, 848, 854, 850, 875, and 2239 nm) but differ significantly at 2.0 order (2239, 1180, 1605, 175 6, 2063, and 1793 nm).

(3) Performance Evaluation of the Dunhuang Mural Plaster Pho sphate Content Prediction Model: When predicting the behavio r of murals under unknown concentration erosion, the 1.9 order model offers the highest inversion accuracy, achieving a maxi mum R^2 value of 0.783 after cross-validation. Empirical tests d emonstrate that the correlation of fractional order differentiatio n exceeds that of integer order, with precision improvements of 9.36% and 39.57% over the integer orders (1.0 and 2.0) respect ively. This study has successfully developed a hyperspectral fea ture inversion model for predicting Mural Plaster phosphate co ntent based on the FOD method, exhibiting high efficiency and accuracy in the assessment of salt damage in Dunhuang murals (Figure 9, Table 3).

This contribution has been peer-reviewed. The double-blind peer-review was conducted on the basis of the full paper.
https://doi.org/10.5194/isprs-annals-X-2-2024-201-2024 | © Author(s) 2024. CC BY 4.0 License.

REFERENCES

Sun, Tongxin, et al., 2023: Restoring Dunhuang Murals: Craftin g Cultural Heritage Preservation Knowledge into Immersive Vi rtual Reality Experience Design.*International Journal of Huma n–Computer Interaction*., 1-22. doi.org/10.1080/10447318.202 3.2232976

Wang,F., Peng,S., Fan,L., Li,Y., 2022: Mechanism of pore relati ve humidity on salt swelling characteristics in sulfate saline soil. *Alexandria Engineering Journal.*, 61 (6),4963-4976. doi.org/1 0.1016/j.aej.2021.09.062.

Sharma, Anjali, Manager Rajdeo Singh, and Rajat Jangid., 202 3: Scientific study of the pigments and binders used in mural pa inting from the 16th-century ce St Mary's Church of Cheriapall y, Kottyam, Kerala, and its relevance to conservation.*Archaeom etry* 65.3 617-634. doi.org/10.1111/arcm.12836.

Scrivano,S., Gaggero,L., 2020: An experimental investigation i nto the salt-weathering susceptibility of building limestones. *Ro ck Mechanics and Rock Engineering.*, 53,5329-5343.doi.org/10. 1007/s00603-020-02208-x.

Li D.,Hu Q.,Ruan S.,et al. 2023: Utilizing Hyperspectral Reflec tance and Machine Learning Algorithms for Non-Destructive E stimation of Chlorophyll Content in Citrus Leaves. *Remote Sen sing.*, 15 (20): 4934. doi.org/10.1021/10.3390/rs15204934.

Peng W.,Beggio G.,Pivato A.,et al. 2022: Applications of near i nfrared spectroscopy and hyperspectral imaging techniques in a naerobic digestion of bio-wastes: A review. *Renewable and Sust ainable Energy Reviews.*, 165: 112608. doi.org/10.1016/j.rser.2 022.112608.

Schodlok M C.,Frei M,Segl K., 2022: Implications of new hype rspectral satellites for raw materials exploration. *Mineral Econ omics.*, 35 (3-4): 495-502. doi.org/10.1007/s13563-022-00327- 1.

Ma J.,Zheng B.,He Y. 2022: Applications of a hyperspectral im aging system used to estimate wheat grain protein: A review. *Fr ontiers in Plant Science.*, 13: 837200. doi.org/10.3389/fpls.202 2.837200.

Wang, Libing, et al. 2021: Estimation of soil salt and ion conten ts based on hyperspectral remote sensing data: A case study of baidunzi basin, China. *Water* 13.4 559.doi.org/10.3390/w13040 559.

J. Chen, P. Jönsson, M. Tamura, Z. Gu, B. Matsushita, and L. E klundh. 2004: A simple method for reconstructing a high-qualit y NDVI time-series data set based on the Savitzky–Golay filter. *Remote sensing of Environment*. 91, 332-344, doi.org/10.1016/ j.rse.2004.03.014.

Guo Zhouqian.,Lv Shuqiang.,et al. 2023: Inversion of salt conte nt in simulated mural based on Hyperspectral mural salt index. *Spectroscopy and Spectral Analysis.*, 43 (10): 3272-3279. doi.o rg/10. 3964/j.issn.1000-0593 (2023)10-3272-08.

Mehmood, Tahir, Solve Sæbø, and Kristian Hovde Liland. 2020: Comparison of variable selection methods in partial least squar es regression.*Journal of Chemometrics* 34.6 e3226.doi.org/10.1 002/cem.3226.

Zhong,Q.,Eziz,M.,Sawut,R.,Ainiwaer,M.,Li,H.,& Wang,L., 202 3: Application of a Hyperspectral Remote Sensing Model for th e Inversion of Nickel Content in Urban Soil.*Sustainability.*, 15 (18),13948. doi.org/10.3390/su151813948.

Hou,Y., Zhang,F., 2014: Estimation model of desert soil organi c matter content using hyperspectral data.*Transactions of the C hinese Society of Agricultural Engineering.*, 30 (16),113-120.

.

Fu,Cheng-Biao.,Hei-Gang Xiong., An-Hong Tian,. 2019: Study on the effect of fractional derivative on the hyperspectral data of soil organic matter content in arid region.*Journal of Spectros copy*., doi.org/10.1115/2019/7159317.

Sousa,J., Vanterler da C., Kishor D.,. Kucche., E. Capelas De O liveira,. 2019: Stability of ψ-Hilfer impulsive fractional differen tial equations.*Applied Mathematics Letters.,* 88,73-80. doi.org/ 10.1016/j.aml.2018.08.013.

Zhou, Ping, Jun Ma, and Jun Tang. 2020: Clarify the physical p rocess for fractional dynamical systems.*Nonlinear Dynamics* 1 00 2353-2364.doi.org/10.1007/s11071-020-05637-z.

Sousa,J., Kucche,K., De,O., 2019: Stability of ψ-Hilfer impulsi ve fractional-order differential equations. *Applied Mathematics Letters*., 88,73–80. doi.org/10.1016/j.aml.2018.08.013

Abbas,S., Benchohra,M., Lazreg,J., Zhou,Y., 2017: A survey on Hadamard and Hilfer fractional-order differential equations: A nalysis and stability. *Chaos Solitons Fractals.*, 102,47–71. doi.o rg/10.1016/j.chaos.2017.03.010.

Y. Yan et al., 2022: Non-destructive testing of composite fiber materials with hyperspectral imaging—Evaluative studies in th e EU H2020 FibreEUse project. *IEEE Transactions on Instrum entation and Measurement.* 71, 1-13, doi.org/10.1109/TIM.202 2.3155745.

Hong,Y., Liu,Y., Chen,Y., Liu,Y., Yu,L., Liu,Y., 2019: Cheng,H. Application of fractional-order differential in the quantitative e stimation of soil organic matter content through visible and nea r-infrared spectroscopy. *Geoderma.*, 337,758–769. doi.org/10.1 016/j.geoderma.2018.10.025

Wang,X., Zhang,F., Kung,H.-T., 2018: Johnson,V.C. New meth ods for improving the remote sensing estimation of soil organic matter content (SOMC) in the Ebinur Lake Wetland National Nature Reserve (ELWNNR) in northwest China. *Remote Sens. Environ*., 2018,218,104–118. doi.org/10.1016/j.rse.2018.09.020.

Bi,W. 2022: Study on coupled heat and mass transfer process a nd characteristics of earthen plasters in Mogao Grottoes. *Doctor, Xi’an University of Architecture and Technology.*, doi.org/10.27 393/d.cnki.gxazu.2022.000010.

Karaca, Yeliz, and Dumitru Baleanu. 2022: Evolutionary Mathe matical Science, Fractional Modeling and Artificial Intelligence of Nonlinear Dynamics in Complex Systems.*Chaos Theory an d Applications* 4.3 111-118.

Wang,X., Zhang,F., Kung,H. T., Johnson,V. C., Latif,A., 2020: Extracting soil salinization information with a fractional-order f iltering algorithm and grid-search support vector machine (GS-SVM) model.*International Journal of Remote Sensing*,41 (3),9 53-973. doi.org/10.1080/01431161.2019.1654142.

Tian,A., Zhao,J., Tang,B., Zhu,D., Fu,C., Xiong,H., 2021: Hype rspectral prediction of soil total salt content by different disturb ance degree under a fractional-order differential model with dif fering spectral transformations.*Remote Sensing*., 13 (21),4283. doi.org/10.3390/rs13214283.

Song,G., Wang,Q., Jin,J., 2023: Fractional-Order Derivative Sp ectral Transformations Improved Partial Least Squares Regressi on Estimation of Photosynthetic Capacity from Hyperspectral Reflectance.*IEEE Transactions on Geoscience and Remote Sen sing*., doi.org/10.1109/TGRS.2023.3270892.

Zhang, J., Jing, X., Song, X., Zhang, T., Duan,W., Su, J., 2023: Hyperspectral estimation of wheat stripe rust using fractional or der differential equations and Gaussian process methods.*Comp uters and Electronics in Agriculture.*,206, 107671. doi.org/10.1 016/j.compag.2023.107671.